Mon. Not. R. Astron. Soc. **322**, 141–148 (2001)

Effect of telescope vibrations upon high angular resolution imaging

S. Altarac,[1] P. Berlioz-Arthaud,[1★] E. Thiébaut,[1★] R. Foy,[1★] Y. Y. Balega,[2★] J. C. Dainty[3★] and J. J. Fuensalida[4★]

[1]*CRAL-Observatoire de Lyon, 9 avenue Charles André 69561 Saint Genis Laval cedex, France*
[2]*Special Astrophysical Observatory, Nizhnij Arkhyz Karachai-Cirkasia 357 147, Russia*
[3]*Blackett Laboratory Optics Section, Imperial College, London SW7 2BZ*
[4]*Instituto de Astrofisica, c/Via Lactea s/n 38200 La Laguna, Tenerife, Spain*

Accepted 2000 October 2. Received 2000 September 21; in original form 2000 May 6

ABSTRACT

We have analysed short-exposure high-resolution images obtained on the William Herschel Telescope (WHT), Big Telescope Azimuthal (BTA) and Canada–France–Hawaii Telescope (CFHT) in order to investigate mechanical vibrations that are capable of reducing the high angular resolution allowed by speckle-interferometric methods. After filtering the photon noise we have computed power spectra of the image centres of gravity. In these spectra we have found vibration features that differ from one telescope to another and that vary in particular with the zenith angle. In the case of the WHT we discuss these results in terms of possible causes and in terms of degradation of the transfer function. We present some means to improve the data.

Key words: atmospheric effects – instrumentation: high angular resolution – methods: data analysis – techniques: high angular resolution – techniques: image processing – telescopes.

1 INTRODUCTION

Telescope motions are negligible for long-time exposures in comparison with the scale of the seeing disc, i.e. λ/r_0. Speckle-interferometric methods (Labeyrie 1970) aim at recovering diffraction-limited images. If the image displacement during a short exposure image (frame) is not negligible with respect to the diffraction pattern then speckle interferometry is unable to correct it and a degradation of the point spread function (PSF) is observed. Such displacements are not isotropic and may lead to spurious asymmetry measurements, especially if vibrations are time-dependent and affect differently the programme object and the reference object for the PSF (Thiébaut et al. 1995; Kibblewhite & Chun 1998). In this Paper we show that such effects are significant at the three large telescopes where we have run speckle interferometry observations. We present a complete analysis for the William Herschel Telescope (WHT) and also show the presence of this phenomenon for the Big Telescope Azimuthal (BTA) and the Canada–France–Hawaii Telescope (CFHT). We then discuss the effect of these vibrations on the transfer function and how to reduce their effects either by debiasing our data or at least by rejecting the most seriously affected frames.

★ E-mail: pberlioz@obs.univ-lyon1.fr (PBA); thiebaut@obs.univ-lyon1.fr (ET); foy@obs.univ-lyon1.fr (RF); balega@sao.ru (YYB); c.dainty@ic.ac.uk (JCD); jjf@ll.iac.es (JJF)

2 DATA AND REDUCTION

2.1 Origin of data

In this study we used speckle-interferometry observations of χ Cygni, DF Tau and their references at visible wavelengths obtained with our specklegraph (Foy 1988b) and our photon counting detector CP40 (Foy 1998a). Observations were performed at

(i) the 4.2-m WHT,
(ii) the 6-m BTA of the Special Astrophysical Observatory (SAO),
(iii) the 3.6-m CFHT.

The BTA and WHT are alt–az mounted while the CFHT has an equatorial mount. The journal of observations is given in Table 1.

The exposure time for each frame is 20 ms and the frame number for one sequence is about $1–4 \times 10^4$ with about 10–400 photons per frame. The faint number of photons per frame is a consequence of the faint magnitude of the star (DF Tau and its reference) and of the narrow bandwidth ($\approx$60 Å for χ Cygni and its reference).

2.2 Reduction

Different bias sources arising from the instrument and the detector affect the data. Data preprocessing consists of removing spurious photon detections and parasitic reflections and correcting the photon coordinates for geometrical distortion (Thiébaut 1997).

Then the coordinates of each image barycentre are computed. All the information we need here is the temporal evolution of the image barycentre (see Fig. 1). The effects of telescope guiding commands are manifested in Fig. 1 by the successive slopes.

At the CFHT the abscissae axis corresponds to the declination axis and the ordinates axis to the ascension axis. For alt–az telescopes the orientation of the detector with respect to the telescope axis is a function of the altitude of the star. At the WHT for all our observations the abscissae of the image correspond approximately to the telescope altitude and the ordinates to the azimuth because the angle hours are always less than 20°. For the same reason at the BTA the abscissae of our images correspond approximately to the telescope azimuth and the ordinates to the altitude. In the following we consider that the image axes correspond to the telescope ones.

Table 1. Journal of observations.

Object	Julian Day (24 0000+)	number of frames	ϕ	notes
WHT				
HR 7535 (1)	9137.6388	35092	426	χ Cygni ref.
χ Cygni	9137.6861	42580	372	transit
HR 7535 (2)	9138.6708	43789	175	
HR 7535 (3)	9138.6808	39730	195	transit
BTA				
χ Cygni (1)	9225.3375	51510	154	90 min after transit
χ Cygni (2)	9225.3764	43264	77	
HR 7535	9225.4069	30326	549	χ Cygni ref.
CFHT				
DF Tau	7833.0951	16783	12	
ref. DF Tau	7833.1285	23520	22	

ϕ: mean number of photons per frame.

3 VIBRATION SPECTRA

Discrete Fourier transformation is a suitable method for analysing the frequency content of signals. As a result of photon fluctuation the resulting power spectra are, however, very noisy. We have used wavelet packets to optimize in particular the detection of the variability of vibrations in frequency or amplitude.

3.1 Noise level

Hoyng (1976) derived the expected value $E(S_\nu)$ and the variance σ_ν^2 at a frequency ν of a power spectrum, S_ν, computed with data f_k sampled at a fixed period, defined as

$$S_\nu = \frac{1}{N}\sum_{k,l=0}^{N-1} f_k f_l \exp\left(\mathrm{i}2\pi\nu\frac{k-l}{N}\right), \tag{1}$$

$$E(S_\nu) = s_\nu + 4\sigma_\mathrm{d}^2, \tag{2}$$

$$\sigma_\nu^2 = \sigma_\mathrm{d}^4 + 2s_\nu\sigma_\mathrm{d}^2, \tag{3}$$

where s_ν is the power spectrum obtained with noise-free data, σ_d the data standard deviation, and N the number of samples.

According to equation (2) the noise-free signal energy S_ν is increased by a term proportional to the noise variance in the sampled data: we have to take it in account to restore the data. The variance of the power spectrum (equation 3) is the sum of a white-noise term plus a signal-dependent term. The variance of the image barycentre is related to the photon noise, but it is also a function of the image spread (the distribution of which is not merely Gaussian). To estimate this variance, we have simulated Kolmogorov phase screens by the 'mid-point' algorithm (Lane, Glindemann & Dainty 1992) with different values of the Fried parameter r_0. The Fourier transform of the product of these phase screens with a circular pupil with central obscuration gives the image distribution. We then apply a Poisson transform to simulate

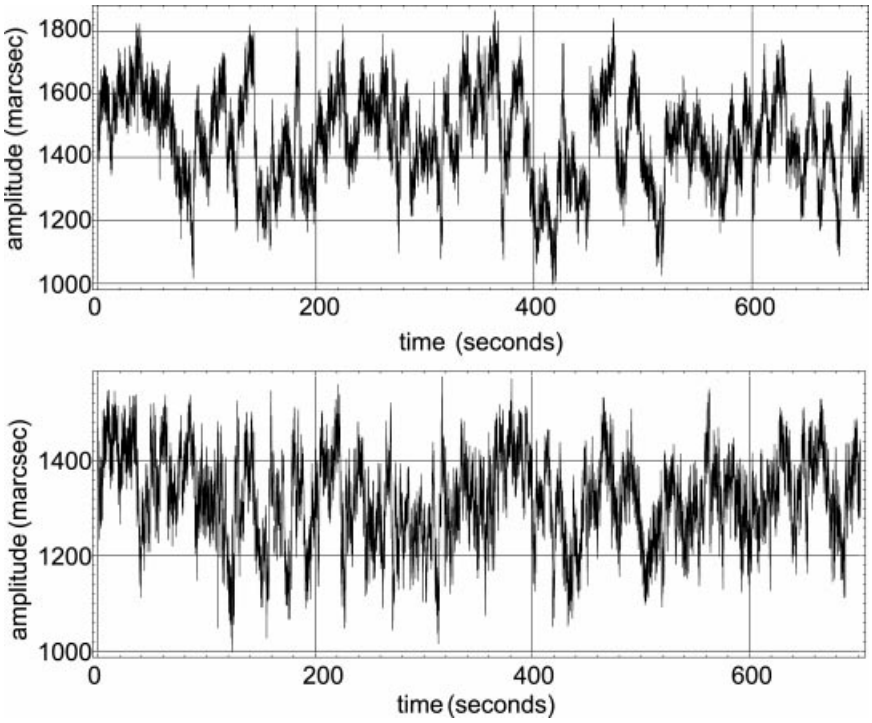

Figure 1. Evolution of the image barycentre position, in altitude (top) and in azimuth (bottom), versus time for the WHT [HR 7535 (1)].

the random photoevents and we then process as for real data. The resulting power spectrum is flat in high frequencies, and the level of this spectrum is flux-dependent. In this case, the temporal dependence of the atmospheric turbulence is not simulated, each successive phase screen being randomly constructed.

3.2 Filtering method

We used the wavelet *àtrou* (with hole) algorithm to filter out the noise of our power spectra. Indeed this method has proven to efficiently recover significant structures in very noisy data (see for example Starck, Siebenmorgen & Gredel 1997).

The wavelet *àtrou* transform of S_ν is the decomposition of the original signal at different local scales

$$S_\nu = C_n(\nu) + \sum_{k=1}^{n} W_k(\nu), \tag{4}$$

where the wavelet coefficients at scale $k \geqslant 1$ are

$$W_k(\nu) = C_{k-1}(\nu) - C_k(\nu). \tag{5}$$

The $C_k(\nu)$ are obtained for each scale by

$$C_0(\nu) = S_\nu \quad \text{and} \quad C_{k+1}(\nu) = \sum_{j=-m}^{m} H_j C_k(\nu + 2^k j\delta\nu),$$

which can be seen as a convolution with the so-called *àtrou* function $H(\nu)$ dilated from one scale to another; $\delta\nu$ is the sampling step.

The wavelet-filtered signal is

$$\tilde{S}_\nu = C_n(\nu) + \sum_{k=1}^{n} \Phi_k[W_k(\nu)]. \tag{6}$$

Following Starck et al. (1997), we used the *àtrou* function ($m = 2$) such that

$$H_0 = \frac{6}{16}, \quad H_{\pm1} = \frac{4}{16}, \quad \text{and} \quad H_{\pm2} = \frac{1}{16},$$

and we chose a filter $\Phi_k(w)$ that cancels all non-significant wavelet coefficients

$$\Phi_k(w) = \begin{cases} w & \text{if } |w| \geqslant \varepsilon_k, \\ 0 & \text{otherwise,} \end{cases} \tag{7}$$

where the threshold ε_k is taken to be 3–5 times the estimated wavelet variance at scale k.

In order to assert the effectiveness of the filtering method, we added a sinusoidal component to a real sequence of data: we were able to detect this additional signal with an amplitude of 2.25 mas and a duration of a tenth of the sequence.

4 INTERPRETATION

Typical spectra observed with the BTA, the WHT and the CFHT are shown in Figs 2, 3 and 4, respectively. The cut-off frequency is 25 Hz as a result of the 50-Hz time sampling.

They show three main features: a continuous decrease of the power with increasing ν at low frequencies (resulting from atmospheric tilt), a flat spectrum from $\approx$4 Hz up to the cut-off frequency (owing to the random arrival of photons) and superimposed narrow and broad lines (as a result of the telescope motions).

4.1 Effect of turbulence and atmospheric tilt

The random arrival of photons, also called *photon noise*, is filtered with appropriate methods and the flat level beyond 6 Hz is its signature.

Atmospheric turbulence has been analysed in different ways; here we are interested with the temporal evolution of the image motion or angle of arrival due to the temporal evolution of the turbulence. Conan, Rousset & Madec (1995) derived the temporal power spectra of the angle of arrival with the hypothesis either of a single or multiturbulent layer. Each layer is modelled by a phase screen translated by the wind. The asymptotic law of the power spectra is proportional to $\nu^{-2/3}$ below a cut-off frequency of V/D

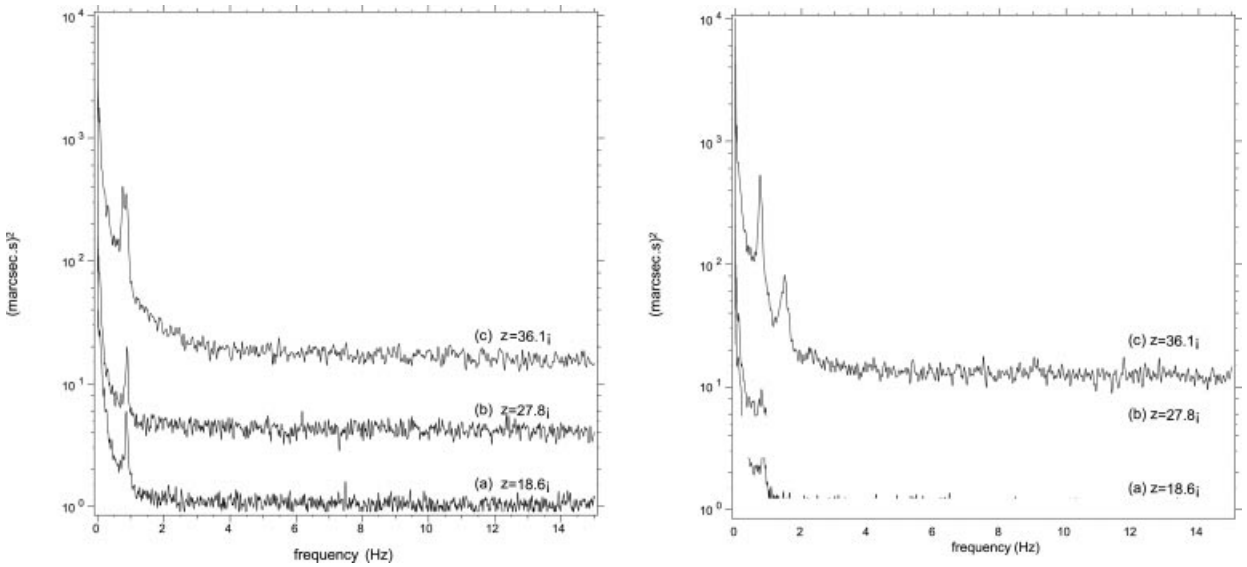

Figure 2. BTA: wavelet-filtered azimuth (left) and altitude (right) power spectra; (a) χ Cygni (1); (b) χ Cygni (2); (c) HR 7535. They have been shifted for clarity.

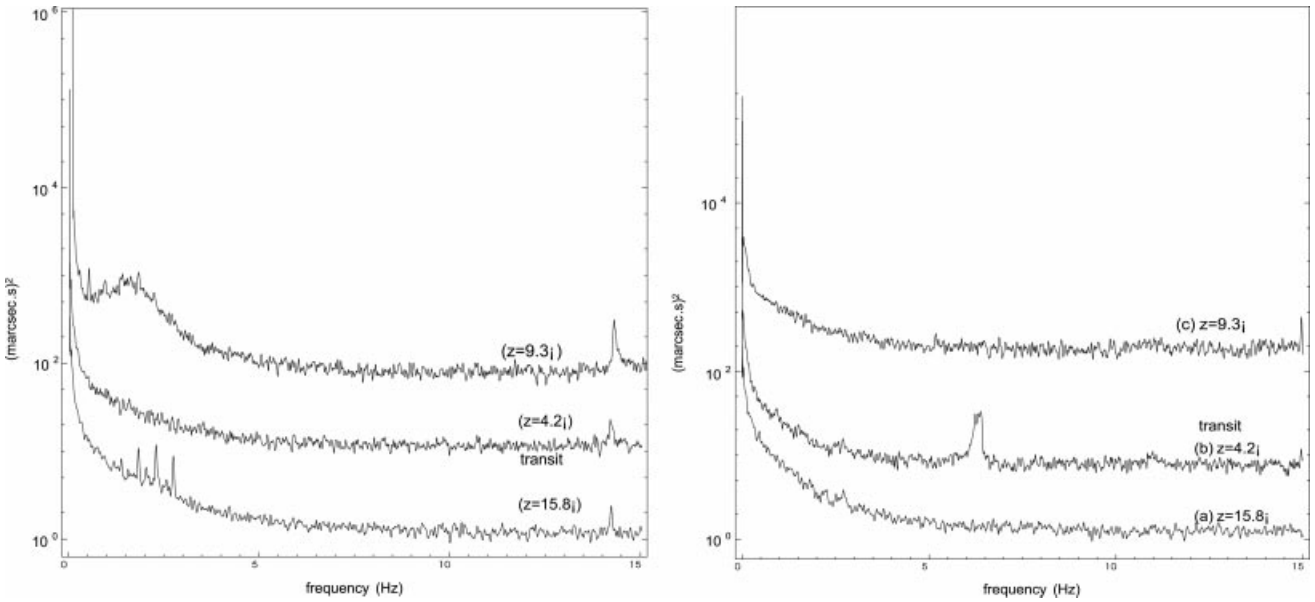

Figure 3. WHT: wavelet-filtered altitude (left) and azimuth (right) power spectra; (a) HR 7535 (1); (b) χ Cygni; (c) HR 7535 (2). They have been shifted for clarity. Transit is marked by line at 6 Hz for the azimuth and by the disappearance of the low-frequency peaks for the altitude.

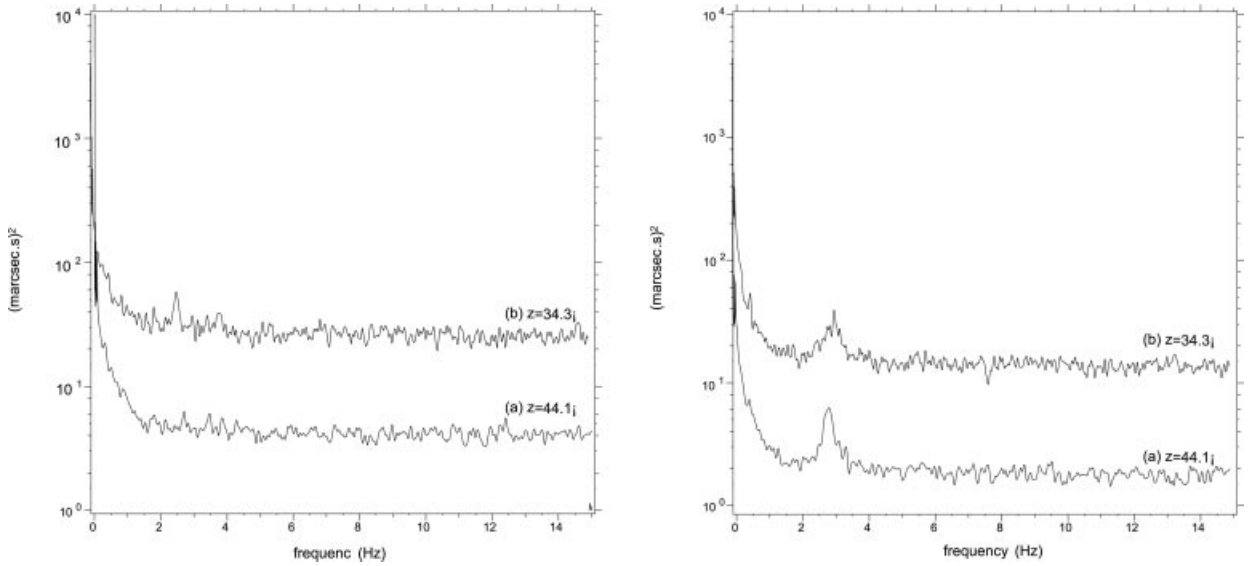

Figure 4. CFHT: wavelet-filtered declination (left) and right ascension (right) power spectra; (a) DF Tau; (b) ref. DF Tau. They have been shifted for clarity.

(with V the wind velocity, and D the telescope diameter) and to $\nu^{-11/3}$ above this frequency.

None of these two effects can produce the lines in the spectra. In the next section, we will prove that the lines in the spectra are due to a mechanical phenomenon.

4.2 Telescope motions

The spectra obtained at the three telescopes show important differences.

The BTA spectra (Fig. 2) are similar in both axes and show a strong narrow line at a fixed frequency of $\approx$0.75 Hz and with a variable amplitude. This feature has already been pointed out by Afanasjev et al. (1988). At the largest zenith distance (i.e. the largest zenithal velocity), in azimuth the 0.75-Hz line has a double peak profile, and in altitude a second line at $\approx$1.5 Hz appears (which is possibly an overtone).

The WHT spectra (Fig. 3) are different from one sequence to another. Most of the altitude spectra have a bump in the 0.5–3.5-Hz band or three evenly spaced lines that are not visible on the azimuth spectra. There are lines at $\approx$0.45, 0.9, 1.35, 1.8, 2.2 and 2.7 Hz. However, some azimuth spectra show strong lines, the frequency of which are rapidly variable (e.g. the 6-Hz peak close to transit). Finally, a line at $\approx$14 Hz is almost always visible on the altitude spectra. Fig. 5 shows the average of the speed power spectrum for the whole sequence. As noise is integrated at high frequencies, it is better to obtain any result to consider the difference between the azimuthal speed and the zenithal speed. Indeed, we can say that the turbulence is isotropic and there are

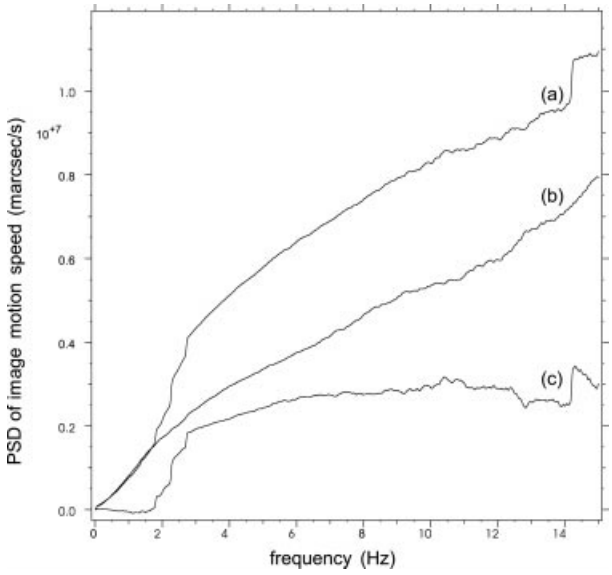

Figure 5. WHT: χ Cygni. Sum of the speed image motion over the whole sequence; (a): V_z, zenithal speed; (b): V_a, azimuthal speed; (c): $V_z - V_a$.

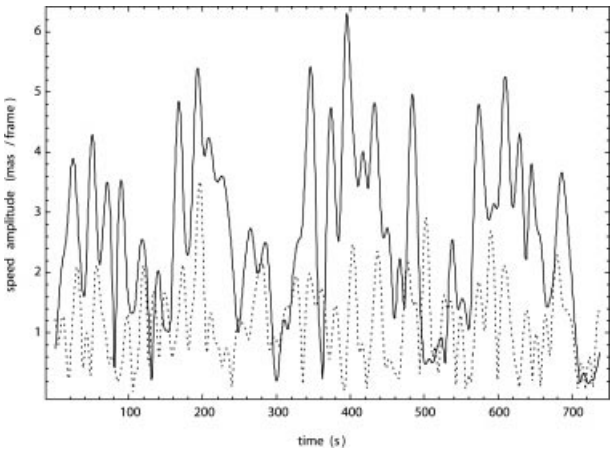

Figure 6. WHT: HR 7535 (1), amplitude of the motion per frame for the 1.8-Hz vibration (solid line: azimuth, dashed line: altitude).

telescope vibrations only on the zenithal axis. The difference characterizes the telescope influence.

4.3 Vibration amplitudes

Now we are interested in measuring the effect of these mechanical vibrations on the image spatial resolution. Let us consider the spectrum obtained at the WHT for HR 7535 (1) the reference of χ Cygni (first sequence). It shows three lines between 1.8 and 2.8 Hz evenly spaced like overtones. We note that there is a second set of weakest evenly spaced lines shifted by $\approx$0.25 Hz. Wilson et al. (1999) have also reported that the low-frequency domain of the power spectrum shows a line at $\approx$2.7 Hz. It is worthwhile noting that their fig. 12 shows additional lines at $\approx$0.5, 0.95 and 1.3 Hz, in good agreement with our spectra. They are weaker and barely visible in particular owing to the log scale in abscissa of their figure.

Then, we have determined the image displacements induced by these three frequencies in our spectra. We have isolated one line from the whole spectrum by filtering it with a rectangular box

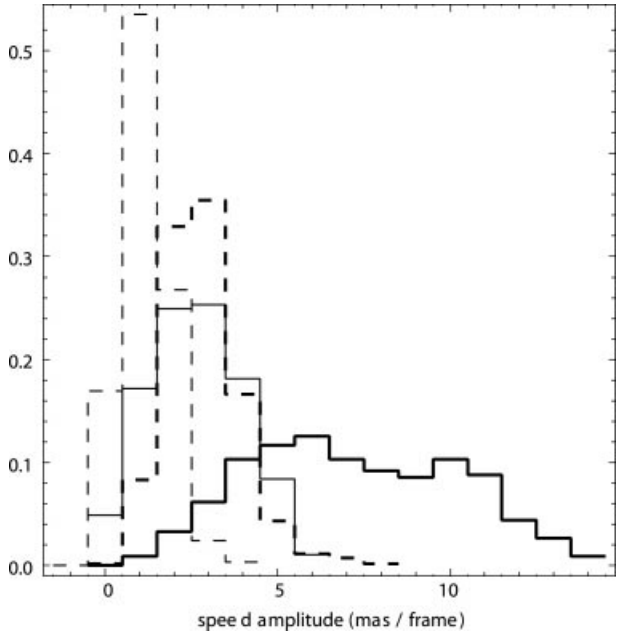

Figure 7. WHT: HR 7535 (1), histogram of amplitude of the motion per frame. Thin lines: 1.8-Hz vibration; thick lines: 1.8-, 2.25- and 2.7-Hz vibrations; solid line: azimuth; dashed line: altitude.

centred on u_0 and with a width of Δu (~the linewidth). Then we have computed the inverse discrete Fourier transform (equation 8).

$$x_k = \frac{1}{N}\sum_u w_u \Phi_u \, \mathrm{e}^{2\mathrm{i}\pi uk/N}, \tag{8}$$

with

$$w_u = \begin{cases} 1 & \text{if } u_0 - \dfrac{\Delta u}{2} \leqslant |u| \leqslant u_0 + \dfrac{\Delta u}{2}, \\ 0 & \text{otherwise.} \end{cases}$$

Fig. 6 shows the maxima and minima envelopes of the maxima of the restored temporal signal corresponding to the 1.8-Hz line for the azimuth and altitude axis. These two envelopes modulate a 1.8-Hz sinusoidal signal, which is not represented.

A peak in the frequency domain is characteristic of an oscillator in the time domain. Its response time is function of the peak shape. If we consider the second peak on the same power spectra of HR 7535 (Fig. 3), we have $\Delta\nu \approx 0.03$ Hz and $\nu \approx 2.2$ Hz. The wave duration is $1/\Delta\nu \approx 33$ s. The period of these oscillations equals $1/\nu \approx 0.45$ s. Now, let us consider the three peaks of the same spectrum. All of them have approximately the same width. The duration of the three oscillations characterized by these frequencies is $\approx$33 s, larger than the oscillation period ($\approx$0.45 s).

The position and speed of an oscillator are

$$x(t) = a\cos(\omega t + \phi) \tag{9}$$

$$v(t) = -a\omega\sin(\omega t + \phi) \tag{10}$$

with amplitude a, pulsation $\omega = 2\pi\nu$, and phase ϕ. Adding the contributions of the three lines, supposing that they are coherent, we obtain the total image displacements. Its amplitude is 44 mas. The maximal speed is $V_{\max} = a\omega$. For the movement at 2 Hz the maximum speed is 0.55 arcsec s^{-1} or 11 mas frame^{-1}. It has to be compared with the Airy disc (λ/D) which equals 24 mas at the observing wavelength (4861 Å), with a 4.2-m telescope. If we

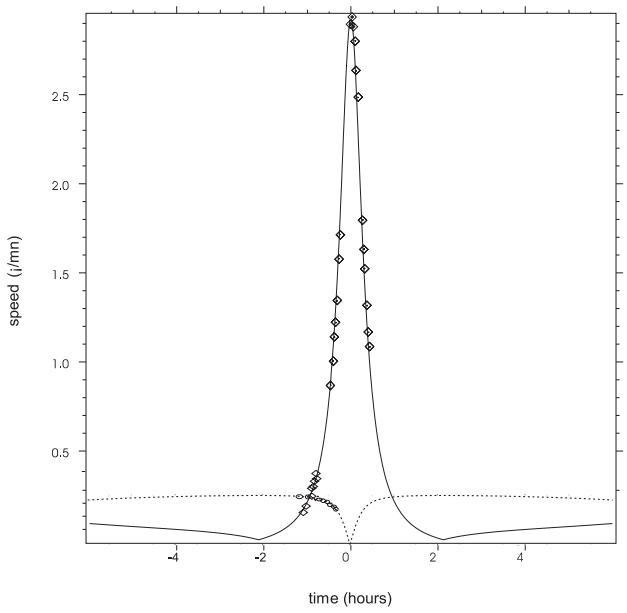

Figure 8. WHT: evolution of frequency values of the ≈6.5-Hz line in the power spectra of HR 7535, versus time (see Fig. 9 and text for details). Diamonds: azimuth; circles: altitude; solid line: theoretical azimuthal speed; dotted line: theoretical zenithal speed.

admit a displacement of 20 per cent of the Airy disc per frame, a speed greater than $\approx 5\,\mathrm{mas\,frame^{-1}}$ will damage the transfer function. The histogram of the amplitude of the motion per frame for the 1.8-Hz band and overtones at 2.25 and 2.7 Hz shows that the average displacement is larger along the azimuth axis (Fig. 7).

4.4 Effect of azimuthal angle on the WHT spectra

We have investigated the time dependence of the spectra obtained at the WHT in relation with the azimuthal and zenithal motions of the telescope. Unlike equatorial mounts, alt–az mounts have variable axial speed when tracking a star. Derivating classical formulae of the alt–azimuthal coordinates in function of the equatorial coordinates leads to the zenithal speed

$$\frac{\mathrm{d}z}{\mathrm{d}t} = \frac{\cos\phi\cos\delta\sin H}{\sin z}\frac{\mathrm{d}H}{\mathrm{d}t}, \tag{11}$$

and the azimuthal speed

$$\frac{\mathrm{d}a}{\mathrm{d}t} = (\sin\phi + \cos\phi\cot z\cos a)\frac{\mathrm{d}H}{\mathrm{d}t}, \tag{12}$$

with ϕ, the site latitude, δ, the object declination, a its azimuth, z its zenithal angle and H, its hour angle.

This speed is maximum at transit. For χ Cygni at the WHT, the zenith distance at transit is $4\overset{\circ}{.}4$, leading to an azimuthal speed of $3\overset{\circ}{.}2\,\mathrm{min^{-1}}$.

To explain the measured frequency variations, we have plotted them versus time. We need a scalefactor to fit the theoretical rotation speed to the measured frequencies.

Fig. 8 shows that the ordinate lines corresponding on the sky to an azimuthal motion are mechanically bound to the rotation of something like a wheel, which performs one revolution per 27 arcsec of azimuthal rotation. The same effect is observable for the zenithal motions: we observe that equally separated lines appeared on the spectra (Fig. 3), corresponding to a fundamental frequency of about 0.45 Hz, which is seen in this figure.

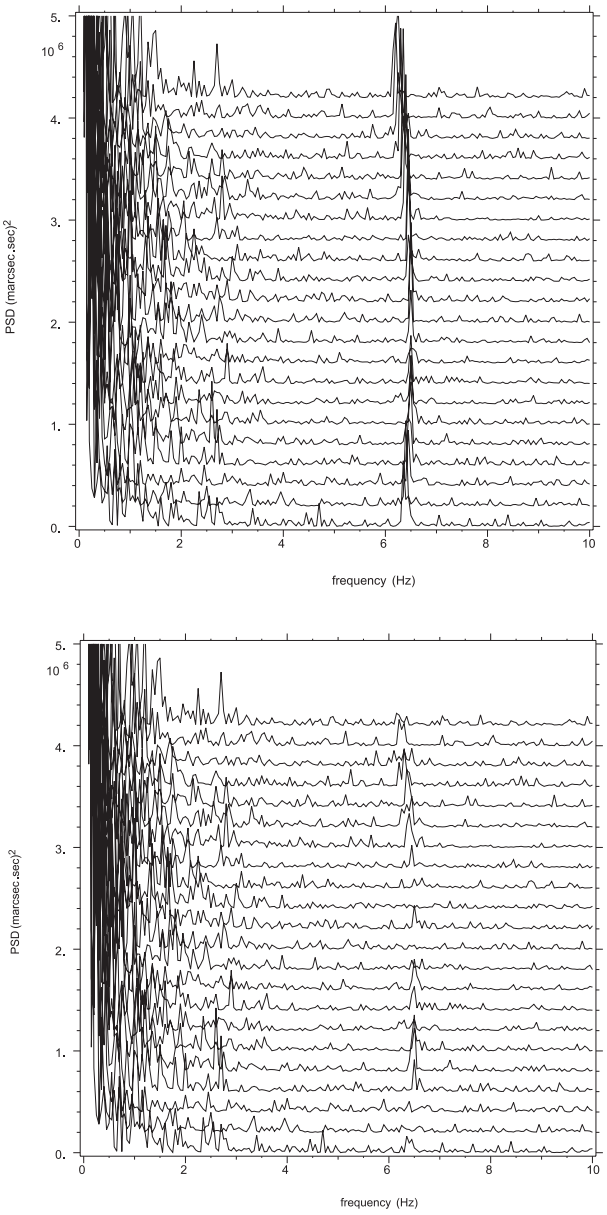

Figure 9. WHT: HR 7535 (3), Power spectra obtained before (top) and after (bottom) subtracting the variable frequency contribution.

Measuring the frequency of the sixth overtone (the highest one that is easily measurable), we have been able to plot the evolution of the vibration frequency around the transit. Here also the measured frequencies fit the theoretical motion and the model of a wheel performing one revolution per 27 arcsec zenithal rotation applies. As a result, the vibration must be coherent, and, knowing the time-dependent frequency, the phase can be fitted on a whole sequence and the amplitude can be estimated by minimizing the variance of the data: Fig. 9 shows the spectra obtained before and after subtracting from the data this variable frequency contribution: the 6-Hz line (also seen in fig. 12 of Wilson et al.) has almost disappeared.

5 DEBIASING DATA

Accounting for the image motion during the exposure Δt, the

mean intensity on the detector becomes

$$i(\boldsymbol{x},t)=\frac{1}{\Delta t}\int_{t'=t-\Delta t/2}^{t'=t+\Delta t/2} i_0[\boldsymbol{x}+\boldsymbol{x}_0(t'),t']\,\mathrm{d}t',$$

where $i_0(\boldsymbol{x},t)$ is the motionless brightness distribution and $\boldsymbol{x}_0(t)$ is the position of the image centroid. Since the exposure time is chosen so as to freeze the turbulence effects, $i_0(\boldsymbol{x},t)$ can be assumed to be constant during Δt. According to the long period of the vibrations (a few seconds) with respect to the short exposure time ($\Delta t \leqslant 20$ ms), one can further assume a constant speed during each exposure

$$i(\boldsymbol{x},t)\simeq\frac{1}{\Delta t}\int_{t'=t-\Delta t/2}^{t'=t+\Delta t/2} i_0[\boldsymbol{x}+\boldsymbol{v}(t)\times t',t]\,\mathrm{d}t',$$

of which the spatial Fourier transform is

$$I(\boldsymbol{u},t)\simeq\mathrm{sinc}[\boldsymbol{u}\cdot\boldsymbol{v}(t)\times\Delta t]I_0(\boldsymbol{u},t),$$

where $I_0(\boldsymbol{u},t)$ is the spatial Fourier transform of $i_0(\boldsymbol{x},t)$ and $\mathrm{sinc}(x)=\sin(\pi x)/\pi x$.

As a result of image motion, the mean power spectrum of short exposure images becomes

$$\langle|I(\boldsymbol{u},t)|^2\rangle\simeq\langle\mathrm{sinc}^2[\boldsymbol{u}\cdot\boldsymbol{v}(t)\times\Delta t]\rangle\langle|I_0(\boldsymbol{u},t)|^2\rangle \qquad (13)$$

where $\langle\cdots\rangle$ denotes time averaging and where we have considered that the velocity of the centroid $\boldsymbol{v}(t)$ due to telescope vibrations/tracking errors is uncorrelated with turbulence effects.

Telescope vibrations result in a linear degradation of the transfer functions of instantaneous images and mean speckle interferometry power spectrum. In principle, analysing the telescope vibrations allows one to estimate $\langle\mathrm{sinc}^2[\boldsymbol{u}\cdot\boldsymbol{v}(t)\times\Delta t]\rangle$ and to obtain the vibrationless power spectrum $\langle|I_0(\boldsymbol{u},t)|^2\rangle$. Fig. 10 shows the attenuation of the modulation transfer function $\langle\mathrm{sinc}^2[\boldsymbol{u}\cdot\boldsymbol{v}(t)\times\Delta t]\rangle$ owing to telescope motions and to the contribution of the atmospheric tilt at the telescope motion

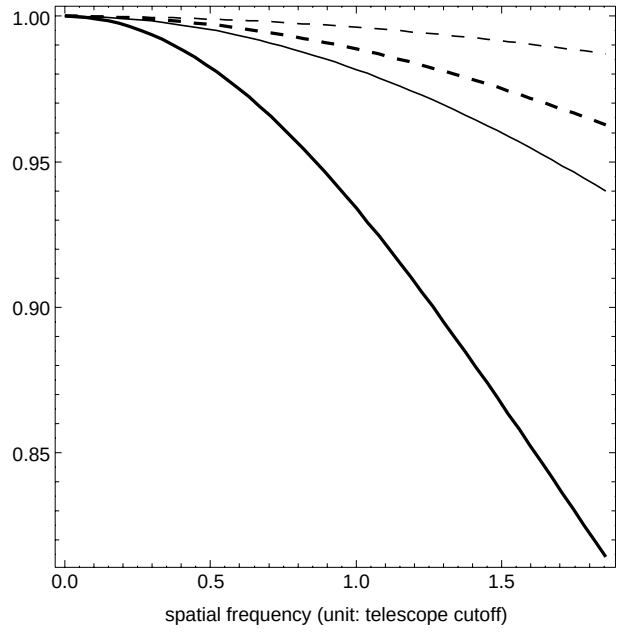

Figure 10. Modulation transfer function due to the frames motion of the WHT data of HR 7535 (1) (same as for Fig. 7). The abscissa is in D/λ units (i.e. diffraction limit). Thin lines: 1.8-Hz vibration; thick lines: 1.8-, 2.25- and 2.7-Hz vibrations; solid line: azimuth; dashed line: altitude.

frequencies: it can be as large as 7 per cent along the abscissa at the diffraction limit and result in an asymmetry with respect to the other axis (for which the attenuation is mainly as a result of the turbulence).

However, vibrations at frequencies higher than 25 Hz or at a signal-to-noise ratio level too low to be detected in our data may be present and yield a much more important degradation than that caused by the only vibration lines taken into account.

6 CONCLUSION

By an appropriate analysis of the data issued from our instrumentation, we have been able to detect and precisely interpret the very weak motions of the telescopes far below their diffracted limited resolution. We expect these results will enhance the reliability of high angular resolution measurements in particular when measuring object asymetries. With these results, we may trust the reliability of our speckle-interferometry data, and enhance the precision of our measurements by selecting the parts of data less affected by telescopes vibrations and by debiasing the PSF. Furthermore, we have developed a method to detect, understand and reduce the vibrations of the existing or future telescopes. Whereas in speckle interferometry the effects of telescope vibrations can be corrected with a tip–tilt mirror or, if we have enough signal, by reducing the exposure time, they are critical for adaptive optics using a polychromatic laser guide star (Foy et al. 1995), which allows the measurement of the atmospheric tilt from a laser guide star without natural guide star, but not to measure the mechanical tilts (Foy et al. 1998; Tokovinin 2000).

ACKNOWLEDGMENTS

This paper is based on observations made with the BTA telescope operated by the Special Astrophysical Observatory of the Academy of Sciences of Russia, with the Canada–France–Hawaii Telescope operated jointly by the Canadian SRC, the French CNRS and the University of Hawaii, and with the William Herschel Telescope operated on the island of La Palma by the Isaac Newton Group in the Spanish Observatorio del Roque de los Muchachos of the Instituto de Astrofisica de Canarias. We thank the staff of the CFHT, BTA and WHT observatories for their support in these observations. The authors participate in the *Laser Guide Star* network of the European Union TMR programme (contract ERBFMRX-CT96-0094).

REFERENCES

Afanasjev V. L., Balega I. I., Balega Y. Y., Vasyuk V. A., Orlov V. G., 1988, in Merkle F., ed., ESO Conf. 29, High-resolution imaging by interferometry. ESO, Garching, p. 127

Conan J.-M., Rousset G., Madec P.-Y., 1995, J. Opt. Soc. Am. A, 12, 1559

Foy R., 1988a, in Robinson L. B., eds, Instrumentation for Ground-Based Optical Astronomy, Present and Future. Springer-Verlag, New York, p. 589

Foy R., 1988b, in Robinson L. B., eds, Instrumentation for Ground-Based Optical Astronomy, Present and Future. Springer-Verlag, New York, p. 345

Foy R., Migus A., Biraben F., Grynberg G., McCullough P. R., Tallon M., 1995, A&AS, 111, 569

Foy R. et al., 1998, in Phipps C., ed., Proc. SPIE Vol. 3343, High-Power Laser Ablation. SPIE, Bellingham, WA, p. 194

Hoyng P., 1976, A&A, 47, 449
Kibblewhite E. J., Chun M. R., 1998, in Bonaccini D., Tyson R. K., eds, Proc. SPIE Vol. 3353, Adaptive Optical System Technologies. SPIE, Bellingham, WA, p. 522
Labeyrie A., 1970, A&A, 6, 85
Lane R. G., Glindemann A., Dainty J. C., 1992, Wave in random media, 2, 209
Starck J.-L., Siebenmorgen R., Gredel R., 1997, ApJ, 482, 1011
Thiébaut E., 1997, J. Opt. Soc. Am. A, 14, 122
Thiébaut E., Balega Y., Balega I., Belkine I., Bouvier J., Foy R., Blazit A., Bonneau D., 1995, A&A, 304, L17
Tokovinin A., 2000, MNRAS, 316, 637
Wilson R. W., O'Mahony N., Packham C., Azzaro M., 1999, MNRAS, 309, 379

This paper has been typeset from a TEX/LATEX file prepared by the author.